

Ultra-narrowband interference circuits enable low-noise and high-rate photon counting for InGaAs/InP avalanche photodiodes

YUANBIN FAN,^{1,†} TINGTING SHI,^{1,2,3,†} WEIJIE JI,¹ LAI ZHOU,¹
YANG JI^{2,3} AND ZHILIANG YUAN^{1,*}

¹Beijing Academy of Quantum Information Sciences, Beijing 100193, China

²State Key Laboratory for Superlattices and Microstructures, Institute of Semiconductors, Chinese Academy of Sciences, Beijing 100083, China

³College of Materials Science and Opto-Electronic Technology, University of Chinese Academy of Sciences, Beijing 100049, China

[†]These authors contributed equally.

*yuanzl@baqis.ac.cn

Abstract: Afterpulsing noise in InGaAs/InP single photon avalanche photodiodes (APDs) is caused by carrier trapping and can be suppressed successfully through limiting the avalanche charge via sub-nanosecond gating. Detection of faint avalanches requires an electronic circuit that is able to effectively remove the gate-induced capacitive response while keeping photon signals intact. Here we demonstrate a novel ultra-narrowband interference circuit (UNIC) that can reject the capacitive response by up to 80 dB per stage with little distortion to avalanche signals. Cascading two UNIC's in a readout circuit, we were able to enable high count rate of up to 700 MC/s and low afterpulsing of 0.5 % at a detection efficiency of 25.3 % for 1.25 GHz sinusoidally gated InGaAs/InP APDs. At -30 °C, we measured 1 % afterpulsing at a detection efficiency of 21.2 %.

Introduction

Semiconductor avalanche photodiodes (APD's) are versatile for weak light detection, with applications from remote ranging [1, 2], quantum communication [3] and fluorescence lifetime imaging [4] to optical time-domain reflectometry [5, 6]. For practical fiber quantum key distribution (QKD), InGaAs/InP APD's are the detector of choice because they are compact and low cost, and allow cryogenic-free or even room-temperature operation [3]. However, they suffer from spurious afterpulsing arising from carrier trapping by defects in the multiplication layer, especially at high detection efficiencies [7, 8]. To minimise afterpulsing, an APD can be biased on for a sub-nanosecond duration only when a photon arrival is expected. In doing so, charge per avalanche can be reduced to the order of 10 fC [9–11], corresponding to a transient current of less than 0.1 mA. Such weak avalanches have to be discriminated through use of a readout circuit that removes the strong capacitive response to the applied gates. Gated InGaAs detectors are capable of counting photons at up to 60% efficiencies [12] and 1 GHz rate [13] and with photon number resolution [14]. Thanks to this success, gating approach has been applied to traditionally free-running Si devices for performance enhancement [15, 16].

Existing readout circuits include band stop [8, 11, 17] or low-pass [12, 18, 19] filtering under sine-wave gating [11], self-differencing [7, 20], and transient reference cancellation [10, 21]. While simple for implementation, frequency filtering distorts the avalanche signals due to its rejection of a sizeable portion of frequency components, thus increasing time jitter and temporal errors in photon registrations [18]. Self-differencing [20] and reference cancellation methods [10] are able to maintain avalanche signal fidelity but may suffer operational complexities. The former requires wideband performance for the entire circuitry and thus inconvenience an adjustable delayline [9] for frequency alignment, while the latter can be unstable because the transient reference is derived separately from the capacitive response.

Here we propose and experimentally demonstrate a simple, low-distortion ultra-narrowband interference circuit (UNIC) that can suppress the capacitive response for a 1.25 GHz gated InGaAs/InP APD single photon detector. The circuit is an asymmetric radio-frequency (RF) interferometer. One of its arms contains a narrow band pass filter (BPF) based on surface acoustic wave resonator (SAW) to retrieve the fundamental wave of the gating signal. The filtered wave then interferes destructively with the same frequency component transmitted via the other arm through a coupling module, thereby eliminating the capacitive response. This interference occurs over the narrow band, so it can provide a broad and continuous pass band in frequency domain to maintain the avalanche signal with little distortion. This allows to achieve ultra-low afterpulsing probabilities and excellent jitter performance at high detection efficiencies from two InGaAs APD's that exhibit capacitive responses of very different amplitudes.

Detector characterisation setup

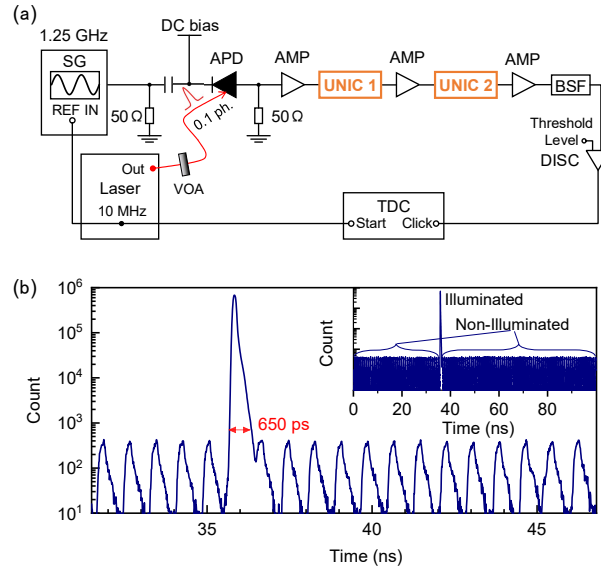


Fig. 1. **(a)** Single-photon characterisation setup for 1.25 GHz sinusoidally gated InGaAs/InP APDs using UNICs for avalanche impulse readout; **(b)** Histogram of the photon detection events measured by the characterisation setup **(a)** on an InGaAs APD detector that was regulated at a temperature of 30 °C. The photon detection peak exhibits a 30 dB width of 650 ps. AMP: amplifier; APD: avalanche photodiode; BSF: band stop filter; DISC: discriminator; SG: signal generator; TDC: time-to-digital converter; UNIC: ultra-narrowband interference circuit; VOA: variable optical attenuator.

Figure 1(a) shows our single photon characterisation setup for InGaAs APDs. A 1550 nm passively mode-locked laser serves as the light source and provides stable short pulses of 0.5 ps duration at a repetition rate of 10 MHz. The laser output power is monitored by an optical power meter (EXFO FTB-1750) and its pulse intensity is set by a variable optical attenuator (VOA, EXFO FTB-3500) to 0.1 photon/pulse at the fiber input of APD under test. It provides a 10 MHz reference to a signal generator (SG) for synthesising a 1.25 GHz sinusoidal wave with up to 27 V voltage swing. In combination of a suitable DC bias, this AC signal periodically gates the APD above its breakdown voltage (60 – 70 V) to achieve single photon sensitivity. The APD output is processed by the readout module consisting of two identical 1.25 GHz UNIC's, one 2.5 GHz band stop filter (BSF), and three RF amplifiers (AMPs). Amplification of the raw APD signals

is useful as it prevents weak avalanche signals from falling below thermal noise by attenuation of the first UNIC. The readout signal is discriminated by a discriminator for avalanches before feeding to a time-digital-converter (TDC) with a dead time of 2 ns for time-resolved photon counting. Figure 1(b) is a typical histogram obtained with this setup.

APD under test is temperature-regulated using their integrated thermal-electric cooler, which is driven by a temperature controller (Thorlabs TED200C). A source-measure unit (Keithley 2635B) provides the DC bias and simultaneously monitors the current flowing through the APD. In characterising the maximum count rate, we replace the 10 MHz laser with a continuous-wave distributed feedback laser (DFB) laser, the output of which is carved into 1.25 GHz, 50 ps pulse train using an intensity modulator. We use a high speed digital oscilloscope to record the detector output and extract the count rate through digital discrimination in software. The oscilloscope method is carefully calibrated at low count rate regimes to be consistent with the hardware discriminated result using the photon counter (Stanford Research SR400).

The setup is able to measure dark count probability, afterpulsing probability, detection efficiency, maximum count rate, avalanche charge and time jitter. With no performance screening, two fiber-pigtailed APDs from different manufacturers were used in this study, named APD#1 and APD#2 respectively.

Ultra-narrowband interference circuit (UNIC)

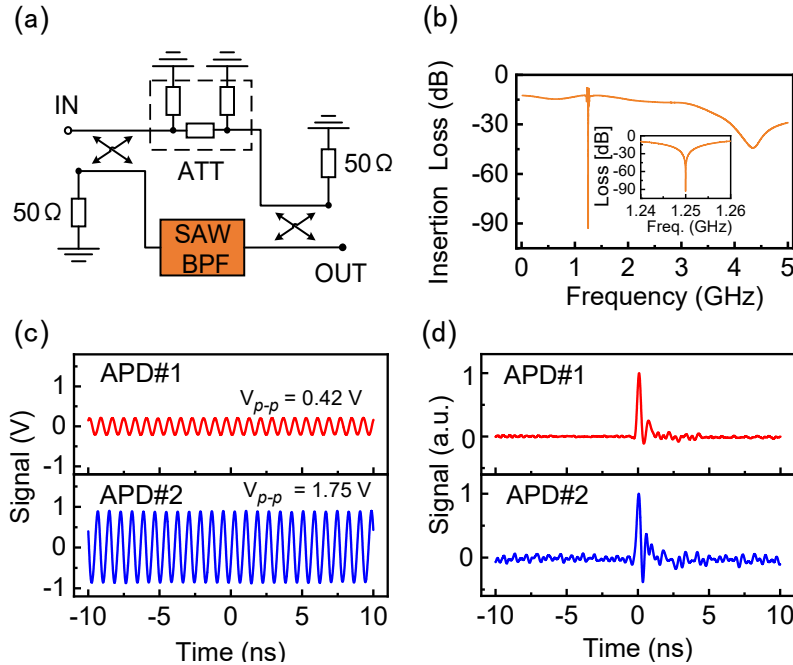


Fig. 2. (a) Schematic for ultranarrow interference circuit (UNIC); (b) Transmission spectrum of a heroic UNIC PCB; Inset: Magnified view for region of 1.24 – 1.26 GHz. (c) Raw capacitive responses from APD#1 (top) and APD#2 (bottom) under identical 27.0 V V_{p-p} gating; (d) Recovered avalanche impulses. ATT: attenuator; SAW BPF: surface acoustic wave band pass filter.

With sub-nanosecond gating, a photon induced avalanche is an impulse and has a wide spectrum. On the other hand, the capacitive response is periodic and has its most energy concentrated at the

gating frequency or its higher harmonics. This spectral difference allows frequency-dependent signal processing to remove the capacitive response and keep the wide-band impulses intact. Figure 2(a) shows a circuit diagram of UNIC. It is an RF interferometer containing two couplers of 9:1 power splitting ratio, a π -resistive attenuator (ATT) and surface acoustic wave band pass filter. Two of the ports are terminated by 50 Ω resistors. The SAW BPF features a central frequency of 1.25 GHz, 20-dB passband of 35 MHz, insertion loss of 3 dB, and group delay of 34 ns. It filters out the fundamental wave of the gating frequency, which then interferes with the APD signal transmitted through the other arm. The attenuation and differential delay are set to enable destructive interference for the 1.25 GHz frequency component at the UNIC output port. The UNIC differential delay (Δt) meets the condition below

$$\Delta t = T_g^{SAW} + \delta t = (N + 1/2)/f_g, \quad (1)$$

where T_g^{SAW} is the group delay of the SAW BPF, δt the delay caused by the track length difference between two arms, $f_g = 1.25$ GHz the APD gating frequency, and N is an integer number. For a compact circuit, we choose δt to be less than the half-wave of the gating signal. With the SAW device used, $N = 42$ and $\delta t = 155$ ps. The resulting UNIC unit has a small footprint of 38×15 mm² on printed circuit boards (PCBs).

The large T_g^{SAW} brings two additional benefits. Firstly, it substantially increases the PCB manufacturing tolerance, as a 0.5 mm deviation in the RF track length will just alter the circuit central frequency by less than 10^{-4} . This eliminates the requirement of an adjustable delayline which is required in a self-differencing circuit for precise frequency alignment. Secondly, it helps to produce an ultra-narrow band rejection at its designed frequency. Figure 2(b) shows the measured transmission spectrum (S21 parameter) of our heroic UNIC PCB, and its inset expands the frequency section of 1.24 – 1.26 GHz to show the narrowness of the insertion loss dip in the close proximity of the resonance frequency of 1.25 GHz. The dip of the heroic (typical) PCB features a loss of -95 dB (-80 dB), representing a suppression of 80 dB (65 dB) as compared with the background loss for other frequencies under 2 GHz. The dip has a 30 dB linewidth of merely 30 kHz, thus ensuring crucial suppression of the APD gating signal without overly distorting the avalanche signals. The background loss of about 14 dB is caused mainly by the 9:1 couplers and can be reduced in future with more balanced splitters.

Cascading two UNIC's enables a stable 100 dB suppression of the primary gating frequency and thus provides sufficient performance redundancy. Their attenuation to the avalanche signal is compensated by using RF amplifiers (Fig. 1(a)). Second order harmonics (2.5 GHz) is suppressed by a band stop filter of conventional LC design. Figure 2(c) shows raw outputs from two different APD's under identical sinusoidal gating. Their respective capacitive responses are measured to be 0.42 V and 1.75 V. Despite their 4 times differences, UNIC's can successfully reject the sinusoidal responses and retrieve avalanches with excellent signal-to-background ratio, as shown in Fig. 2(d). For APD#2, we just adjusted the gain of the first AMP to avoid saturation and distortion.

Results and discussion

Time-resolved photon counting allows precise extraction of the net photon detection efficiency (η_{net}) and the afterpulsing probability (P_A), which is defined as the ratio of the total afterpulses per photon counting event. Figure 1(b) shows a histogram of avalanche events measured for APD#1 under 10 MHz pulsed excitation of 0.1 photon/pulse. The illuminated peak has a full-width of 1/1000 maximum (30 dB width) of just 650 ps, which is shorter than the gating period of 800 ps and thus allows low-error clock number assignment that is essential for high speed QKD. The count at non-illuminated gates arise from detector dark count and afterpulses and is more than 3 orders of magnitude lower than that of the illuminated gate. We extract quantities of P_I and P_{NI} , *i.e.*, the respective counting probabilities for each illuminated and

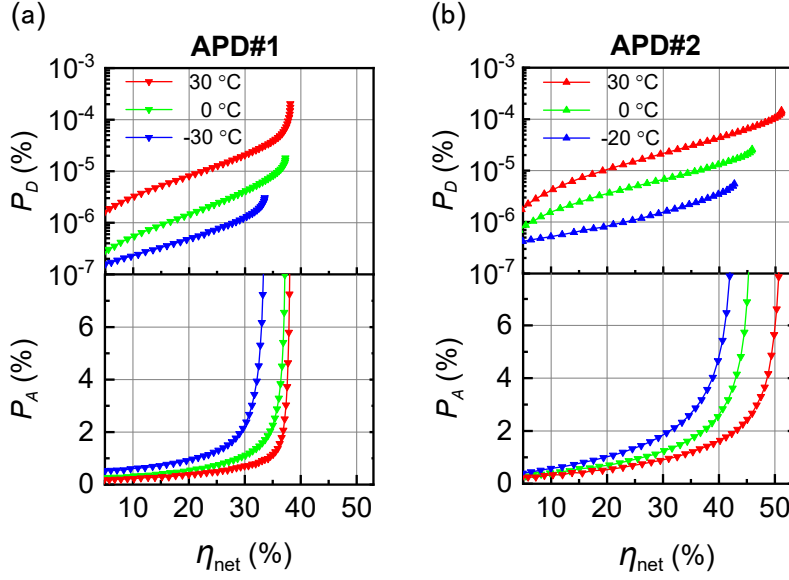


Fig. 3. Dark count probability (top) and afterpulse probability (bottom) as a function of photon detection efficiency of (a) APD#1 and (b) APD#2 measured for several different temperatures.

non-illuminated gate. With a separate measurement of the detector dark count probability (P_D), we calculate the afterpulsing probability using the standard method [17, 20],

$$P_A = \frac{(P_{NI} - P_D) \cdot R}{P_I - P_{NI}}, \quad (2)$$

where $R = 125$ here is the ratio of the gating frequency (1.25 GHz) to the laser illumination (10 MHz). Excluding the dark and afterpulse count probabilities, the net single photon detection efficiency is given by [7]

$$\eta_{net} = \frac{1}{\mu} \ln \frac{1 - P_{NI}}{1 - P_I}, \quad (3)$$

where μ is the average incident photon number per illumination pulse.

Figure 3 shows the characterisation results for APD#1 and APD#2. We fixed the amplitude of the 1.25 GHz sinusoidal signal at 27.0 V, and measured the relevant parameters as a function of the applied direct current (DC) bias, but for clarity the results are plotted as a function of the net detection efficiency (η_{net}). Each device was measured at several different temperatures, while APD#2 could reach only a narrower temperature range due to its cooler compatibility with the temperature control driver. Qualitatively, two devices behave similarly. Both dark count and afterpulsing probabilities increase with photon detection efficiency, and exhibit opposite dependencies on temperature. For both APDs at $\eta_{net} = 30\%$, the afterpulsing probabilities are less than 2.3% at their lowest measurement temperatures with corresponding dark count probabilities of 1.25×10^{-6} and 1.6×10^{-6} for APD#1 (-30 °C) and APD#2 (-20 °C), respectively. Moreover, our UNIC-APDs can offer record low afterpulsing probabilities, as summarised for APD#1 in Figure 4. At -30 °C, APD#1 is able to achieve 5% and 21.2% detection efficiencies at 0.5% and 1.0% afterpulsing probabilities. At these afterpulsing probabilities, the maximum detection efficiency increases with temperature and reaches 25.3% and 34.2% at 30 °C. At 5.9% P_A , APD#2 has a detection efficiency of 50% efficiency at 30 °C and dark count probability of 1.1×10^{-4} .

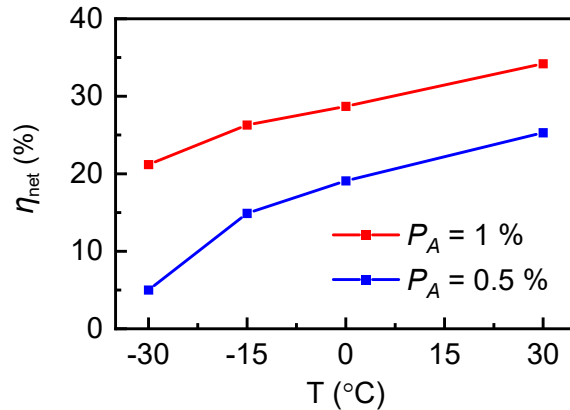


Fig. 4. Temperature dependencies of photon detection efficiency for APD#1 at the given afterpulsing probabilities of 0.5 % (blue) and 1 % (red).

The maximum count rate is a crucial parameter for a number of applications, for example, high bit rate QKD [3] and rapid phase tracking in twin-field QKD [22, 23]. To determine their maximum count rates, we used a DFB laser transmitting at 1.25 GHz as the illumination source and measure the count rate as a function of photon flux. Figure 5 shows an exemplar result obtained from APD#1 at a temperature of 30 °C with its detection efficiency set to 25.3 % in the low flux regime. The detector maintains a linear dependence with incident flux for count rates exceeding 100 MHz, while a maximum count rate of 700 MHz is obtained at the few photons/pulse regime. We attribute the high count rate to the UNIC’s ability of removing the capacitive response and thus allowing discrimination of faint avalanches. From the accompanying current measurement, we extract an avalanche charge of 38 fC, comparable to the best value of 35 fC [9] obtained with the photocurrent measurement method. The ability to detect such weak avalanches ensures low afterpulsing probabilities in our UNIC-APDs. APD#2 was measured to

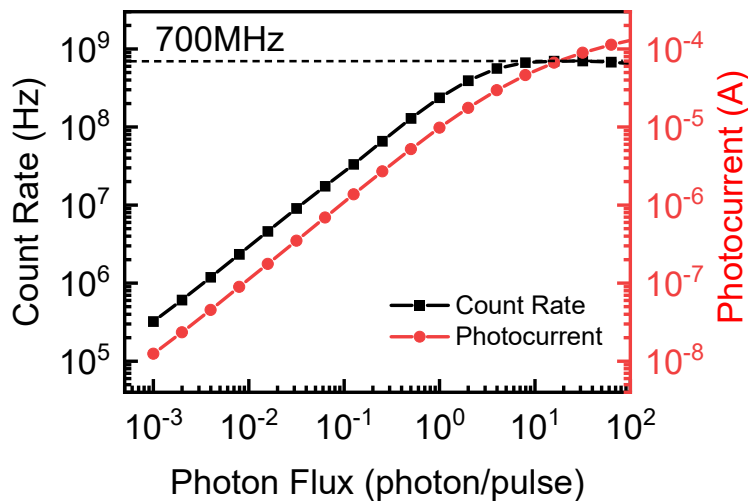


Fig. 5. Maximum count rate (blue) and photoncurrent (red) vs incident flux for APD#1.

have a similar avalanche charge as that of APD#1. When setting its efficiency to 50 %, APD#2's avalanche charge rose to 65 fC due to stronger bias applied. Nevertheless, it was still able to achieve a maximum count rate of 600 MHz.

Table 1. Performance comparison of sub-nanosecond gated InGaAs detectors using different types of readout circuits.

	P_A (%)	η_{net} (%)	P_D (gate ⁻¹)	T (°C)	f_g (GHz)	Readout Method
This work	1.0	21.2	5.4×10^{-7}	-30	1.25	UNIC
He <i>et al</i> [19]	1.0	20.7	7.6×10^{-7}	-30	1.00	low-pass filter + variable width discriminator
Tada <i>et al</i> [8]	1.8	27.7	8×10^{-7}	-35	1.27	band stop filter
Fang <i>et al</i> [12]	2.5	20	1.1×10^{-6}	-30	1.25	low-pass filter
Comandar <i>et al</i> [7]	2.9	20	1.0×10^{-6}	-30	1.00	self-differencing
Liang <i>et al</i> [21]	4.5	20	3.2×10^{-6}	-30	1.25	reference subtraction

Table 1 compares our results with those gigahertz-gated detectors equipped with different readout circuits. For impartiality, we list just data measured at a fixed temperature of -30 °C whenever possible. Here, our UNIC-APD achieved an impressive 1% afterpulsing probability at $\eta_{\text{net}} = 21.2$ %, considerably outperforming most other methods among filtering [8, 12], self-differencing [7] and reference subtraction [21]. In terms of detection efficiency, our result improves marginally over the previous best [19], but which was achieved with help of an uncommon variable width discriminator to mitigate signal distortion by excessive filtering. We attribute the outstanding performance of our detectors to low-distortion signal processing by UNIC's.

It is useful to compare our UNIC-APDs with detectors deployed in QKD systems. In the QKD system optimised for secure key rates (SKRs) [3], the room-temperature self-differencing detectors featured $f_g = 1$ GHz, $\eta_{\text{net}} = 31$ %, $P_A = 4.4$ % and $P_D = 2.25 \times 10^{-4}$ and a SKR of 13.72 Mb/s over a 2 dB channel was obtained. Our UNIC-APD could outperform in all these parameters. At 30 °C and with $P_A = 4.4$ %, APD#2 offers a higher efficiency of 49 % efficiency and twice lower dark count probability of 9.4×10^{-5} , see Fig. 3b. Combined with its high count capability, UNIC detectors are expected to allow a SKR exceeding 25 Mb/s over the same channel loss. This provides an interesting technological path towards 100 Mb/s via wavelength multiplexing.

Conclusion

To summarise, we have developed a novel approach of using UNICs for reading out avalanche signals from 1.25 GHz sinusoidally gated InGaAs APDs. UNIC-APDs were characterised to exhibit excellent performance across the temperature range of -30 – 30 °C, and can offer >20 % detection efficiency at an ultra low afterpulsing probability of 1 %. This performance, together with the circuit's compactness and manufacturing tolerance, will allow UNIC-APDs a considerable potential in QKD applications.

Disclosures. The authors declare that there are no conflicts of interest related to this article.

Data availability. Data underlying the results presented in this paper are not publicly available at this time but may be obtained from the authors upon reasonable request.

References

1. A. Wehr and U. Lohr, "Airborne laser scanning—an introduction and overview," *ISPRS J. Photogramm. & Remote Sens.* **54**, 68–82 (1999).
2. U. Schreiber, A. Schlicht, and K.-H. Haufe, "Systematic biases in laser ranging measurements," *Laser Radar Ranging Atmospheric Lidar Tech. II* **3865**, 64–73 (1999).
3. Z. L. Yuan, A. Plews, R. Takahashi, K. Doi, W. Tam, A. W. Sharpe, A. R. Dixon, E. Lavelle, J. F. Dynes, A. Murakami, M. Kujiraoka, M. Lucamarini, Y. Tanizawa, H. Sato, and A. J. Shields, "10 Mb/s quantum key distribution," *J. Light Technol.* **36**, 3627–3433 (2018).
4. L. Damalakiene, V. Karabanovas, S. Bagdonas, and R. Rotomskis, "Fluorescence-lifetime imaging microscopy for visualization of quantum dots' endocytic pathway," *Int. J. Mol. Sci.* **17** (2016).
5. P. Healey, "Optical time domain reflectometry—a performance comparison of the analogue and photon counting techniques," *Opt. Quant. Electron.* **16**, 267–276 (1984).
6. P. Eraerds, M. Legré, J. Zhang, H. Zbinden, and N. Gisin, "Photon counting OTDR: Advantages and limitations," *J. Light Technol.* **28**, 952–964 (2010).
7. L. C. Comandar, B. Fröhlich, J. F. Dynes, A. W. Sharpe, M. Lucamarini, Z. L. Yuan, R. V. Penty, and A. J. Shields, "Gigahertz-gated InGaAs/InP single-photon detector with detection efficiency exceeding 55% at 1550 nm," *J. Appl. Phys.* **117**, 083109 (2015).
8. A. Tada, N. Namekata, and S. Inoue, "Saturated detection efficiency of single-photon detector based on an InGaAs/InP single-photon avalanche diode gated with a large-amplitude sinusoidal voltage," *Jpn. J. Appl. Phys.* **59**, 072004 (2020).
9. Z. L. Yuan, A. W. Sharpe, J. F. Dynes, A. R. Dixon, and A. J. Shields, "Multi-gigahertz operation of photon counting InGaAs avalanche photodiodes," *Appl. Phys. Lett.* **96**, 071101 (2010).
10. A. Restelli, J. C. Bienfang, and A. L. Migdall, "Single-photon detection efficiency up to 50% at 1310 nm with an InGaAs/InP avalanche diode gated at 1.25 GHz," *Appl. Phys. Lett.* **102**, 141104 (2013).
11. N. Namekata, S. Sasamori, and S. Inoue, "800 MHz single-photon detection at 1550-nm using an InGaAs/InP avalanche photodiode operated with a sine wave gating," *Opt. Express* **51**, 10043–10049 (2006).
12. Y. Q. Fang, W. Chen, T. H. Ao, C. Liu, L. Wang, X. J. Gao, J. Zhang, and J. W. Pan, "InGaAs/InP single-photon detectors with 60% detection efficiency at 1550 nm," *Rev. Sci. Instr.* **91**, 083102 (2020).
13. K. A. Patel, J. F. Dynes, A. W. Sharpe, Z. L. Yuan, R. V. Penty, and A. J. Shields, "Gigacount/second photon detection with InGaAs avalanche photodiodes," *Electron. Lett.* **48**, 111–113 (2012).
14. B. E. Kardynal, Z. L. Yuan, and A. J. Shields, "An avalanche-photodiode-based photon-number-resolving detector," *Nat. Photon.* **2**, 425–428 (2008).
15. O. Thomas, Z. L. Yuan, J. F. Dynes, A. W. Sharpe, and A. J. Shields, "Efficient photon number detection with silicon avalanche photodiodes," *Appl. Phys. Lett.* **97**, 031102 (2010).
16. M. A. Wayne, J. C. Bienfang, and A. L. Migdall, "Low-noise photon counting above 100×10^6 counts per second with a high-efficiency reach-through single-photon avalanche diode system," *Appl. Phys. Lett.* **118**, 134002 (2021).
17. N. Namekata, S. Adachi, and S. Inoue, "1.5 GHz single-photon detection at telecommunication wavelengths using sinusoidally gated InGaAs/InP avalanche photodiode," *Opt. Express* **17**, 6275–6282 (2009).
18. N. Walenta, T. Lunghi, O. Guinnard, R. Houlmann, H. Zbinden, and N. Gisin, "Sine gating detector with simple filtering for low-noise infra-red single photon detection at room temperature," *J. Appl. Phys.* **112**, 063106 (2012).
19. D. Y. He, S. Wang, W. Chen, Z. Q. Yin, Y. J. Qian, Z. Zhou, G. C. Guo, and Z. F. Han, "Sine-wave gating InGaAs/InP single photon detector with ultralow afterpulse," *Appl. Phys. Lett.* **110**, 111104 (2017).
20. Z. L. Yuan, B. E. Kardynal, A. W. Sharpe, and A. J. Shields, "High speed single photon detection in the near infrared," *Appl. Phys. Lett.* **91**, 041114 (2007).
21. Y. Liang, Q. Fei, Z. Liu, K. Huang, and H. Zeng, "Low-noise InGaAs/InP single-photon detector with widely tunable repetition rates," *Photon. Res.* **7**, A1–A6 (2019).
22. M. Lucamarini, Z. L. Yuan, J. F. Dynes, and A. J. Shields, "Overcoming the rate-distance limit of quantum key distribution without using quantum repeater," *Nature* **557**, 400–403 (2018).
23. L. Zhou, J. Lin, Y. Jing, and Z. Yuan, "Twin-field quantum key distribution without optical frequency dissemination," (2022). ArXiv:2208.09347.